Homocysteine impedes neurite outgrowth recovery after intracerebral haemorrhage by downregulating pCAMK2A

Guangyu Guo,[1] Jingfei Yang,[1] Wenliang Guo,[1] Hong Deng,[1] Haihan Yu,[1] Shuang Bai,[1] Gaigai Li,[1] Yingxin Tang,[1] Ping Zhang,[1] Yuming Xu [ID] ,[2,3] Chao Pan,[1] Zhouping Tang [ID] [1]

► Additional supplemental material is published online only. To view, please visit the journal online (http://dx.doi.org/10.1136/svn-2022-002165).

GG and JY are joint first authors.

[1]Department of Neurology, Tongji Hospital of Tongji Medical College of Huazhong University of Science and Technology, Wuhan, Hubei, China
[2]Department of Neurology, The First Affiliated Hospital of Zhengzhou University, Zhengzhou, Henan, China
[3]NHC Key Laboratory of Prevention and Treatment of Cerebrovascular Diseases, Zhengzhou, China

Correspondence to
Dr Zhouping Tang;
ddjtzp@163.com

Dr Chao Pan;
punctualpc@163.com

ABSTRACT

Hyperhomocysteinemia (HHcy) is independently associated with poorer long-term prognosis in patients with intracerebral haemorrhage (ICH); however, the effect and mechanisms of HHcy on ICH are still unclear. Here, we evaluated neurite outgrowth and neurological functional recovery using simulated models of ICH with HHcy in vitro and in vivo. We found that the neurite outgrowth velocity and motor functional recovery in the ICH plus HHcy group were significantly slower than that in the control group, indicating that homocysteine (Hcy) significantly impedes the neurite outgrowth recovery after ICH. Furthermore, phosphoproteomic data and signalome analysis of perihematomal brain tissues suggested that calmodulin-dependent protein kinases 2 (CAMK2) kinase substrate pairs were significantly downregulated in ICH with HHcy compared with autologous blood injection only, both western blot and immunofluorescence staining confirmed this finding. Additionally, upregulation of pCAMK2A significantly increased neurite outgrowth recovery in ICH with HHcy. Collectively, we clarify the mechanism of HHcy-hindered neurite outgrowth recovery, and pCAMK2A may serve as a therapeutic strategy for promoting neurological recovery after ICH.

WHAT IS ALREADY KNOWN ON THIS TOPIC

⇒ Hyperhomocysteinemia (HHcy) is the risk factor for intracerebral haemorrhage (ICH) and is associated with poor prognosis, but its underlying molecular mechanisms affecting neural repair after ICH are still poorly understood.

WHAT THIS STUDY ADDS

⇒ By morphological and behavioural tests, we suggest that Hcy impedes neurite outgrowth and neurological recovery after ICH. Then, our findings further indicate that Hcy significantly downregulates the phosphorylation level of calmodulin-dependent protein kinases 2 (CAMK2A) after ICH, which is associated with neurite outgrowth.

HOW THIS STUDY MIGHT AFFECT RESEARCH, PRACTICE OR POLICY

⇒ Our findings show that pCAMK2A may serve as a key target for promoting neurological recovery after ICH, indicating novel therapeutic strategies for improving the prognosis of ICH with HHcy in the future.

INTRODUCTION

Affecting 2 million people worldwide each year, intracerebral haemorrhage (ICH) is a serious type of stroke, and more than two-thirds of survivors cannot maintain their activities of daily living.[1–3] There are many factors affecting the risk and prognosis of ICH, and high plasma homocysteine (Hcy) concentration, also known as hyperhomocysteinemia (HHcy), is a notable risk factor.[4] According to a recent outpatients cohort of stroke, 35% of them had a high level of plasma Hcy, making it a high concern to this population.[5] In addition, a clinical study showed that HHcy was independently associated with a poorer 3-month clinical outcome in patients with ICH.[6]

Molecular mechanisms that contribute to HHcy-induced disease involve reactive oxygen species and endothelial dysfunction.[7] Endothelial dysfunction may contribute to the increased risk of ICH. However, for most patients with ICH with neurological function dysfunction accompanied by HHcy, whether Hcy directly interferes with neural repair after ICH is unclear. Several studies have revealed that Hcy can perturb phosphoprotein homeostasis,[8 9] and phosphorylation has important implications on the function of neurite outgrowth.[10 11] Therefore, we speculated that Hcy could impede neurite outgrowth and neurological recovery after ICH for patients with HHcy through a disturbance of switch-like kinase-phosphoprotein cascades. To test this hypothesis, we separately constructed ICH with HHcy models in vitro and in vivo. Morphological and behavioural characteristics were measured to evaluate neurite outgrowth recovery and neurological

function. To elucidate the mechanism of Hcy function on neurite outgrowth after ICH at a systemwide level, we used a global phosphoproteomic approach combined with proteomics. We explored the regulation of neurite outgrowth by kinase-substrate signalome and identified the core signalling pathway and target which may serve as a switch-like molecule for neurite outgrowth regulated by Hcy. Finally, we examined and validated its regulatory effect on neurite outgrowth recovery after ICH. Overall, we demonstrate that Hcy can inhibit neurite outgrowth after ICH and identify disturbances in the signalling network caused by Hcy. Importantly, these findings may indicate novel therapeutic strategies for improving the prognosis of ICH with HHcy.

MATERIALS AND METHODS
Animals
Male C57BL/6 mice (aged 5 weeks old, 14–16 g) were used in this study and were provided by the Animal Center of Tongji Hospital of Tongji Medical College of Huazhong University of Science and Technology (Wuhan, China). The mice were housed under a specific temperature-controlled environment with a 12-hour light/12-hour dark cycle. The mice were randomly divided into four groups: (1) Ctrl+vehicle group, (2) HHcy+vehicle group, (3) Ctrl+ICH group and (4) HHcy+ICH group, in which mice in the Ctrl groups were fed an ordinary diet, mice in the HHcy groups were fed with 1.7% high methionine feed for 6 weeks,[12] mice in the ICH groups were stereotactic injected with autologous blood and mice in the vehicle groups were given a sham ICH operation. A total of 220 mice were used for MOST (n: 10×4 = 40), neurobehavioral tests (n: 8×4 = 32), proteome and phosphoproteome (n: 3×3×4 = 36, three mice were mixed for each sample), western blot analysis (n: 8×4 = 32 on days 3, 8×4 = 32 on days 14), immunofluorescence staining (n: 6×4 = 24) and plasma Hcy concentration analysis (n: 6×4 =24). The mice were allowed free access to food and water throughout the experimental period. Six mice died after stereotactic injection with autologous blood.

Plasma Hcy concentration
After the mice were fed 1.7% high methionine feed for 4 and 6 weeks, blood was collected from the inner canthus vein. The concentration of plasma Hcy was measured by the Department of Laboratory Medicine of Wuhan Tongji Hospital.

ICH models
ICH was induced by the stereotactic injection of autologous blood into the basal ganglia as previously described.[13 14] Briefly, male C57BL/6 mice were anaesthetised with pentobarbital sodium and positioned in a stereotaxic frame in a prone position (RWD Life Science, China) and a burr hole was drilled into the skull. Then, 20 µL of autologous blood from the medial canthus vein without any anticoagulants was injected into the right basal ganglia (coordinates 0.5 mm anterior, 2.0 mm lateral

and 3.5 mm ventral to the bregma) at a rate of 1 µL/min by a microinfusion pump (RWD Life Science, China). After injection, the needle was left in position for an additional 10 min to prevent reflux and then withdrawn slowly at a rate of 1 mm/min. After suturing the wounds, all animals were monitored and provided with sufficient food and water. Only mice in which ICH was successful, excluding asymptomatic or dead mice, were included in this study. Using the same dosage as that applied to induce ICH, the mice subjected to the sham operation were only injected with phosphate buffered saline (PBS) into the basal ganglia.

Magnetic resonance imaging
MRI scans were performed to observe the formation and size of the haematoma on the first and third days after the establishment of ICH models. The mice were anaesthetised, fixed with special mouse coils and put into a 3.0 T magnetic resonance machine. The scanning sequence was as follows: coronal position, T2WI, TR 1800 ms, TE 90 ms, 1 mm-thick slice with 0.1 mm interslice gap.

Neurobehavioural tests
All neurobehavioral tests, including modified neurological severity scores (mNSS) and rotarod (Ugo Basile, Comerio, Italy) tests,[15] were blindly administered by a laboratory technician on days 1, 3, 7, 14 and 21. Before inducing ICH, the mice were trained to rotate the rod for three cycles a day with an accelerating rotational speed from 4 rpm to 40 rpm within 5 min for 3 days before the surgical operation. On the third day of training, the average retention time on the rotarod was recorded to obtain baseline latency, and mice with poor motor function were excluded. The retention time of each mouse on the rotarod was tested six times at each time point after the operation, and the maximum value was recorded.

Western blot
Western blot was performed as described previously[16–18] and the mouse brain tissues were separated from the perihematomal region (within 1 mm from the edge of the haematoma) for this analysis. Tissues were lysed and homogenised in RIPA lysis buffer supplemented with PMSF (Beyotime Biotechnology, China). The concentration of total protein in tissues was determined using a bicinchoninic acid (BCA) assay (Beyotime Biotechnology, China). The proteins were separated by 10% sodium dodecyl sulfate polyacrylamide gel electrophoresis (SDS-PAGE) and transferred onto nitrocellulose membranes. Then, the membranes were blocked in 5% skim milk for 1 hour at room temperature and incubated with the following primary antibodies overnight at 4°C: anti-MAP-2 (1:1000, Cell Signaling Technology, USA), anti-synaptophysin (1:5000, Proteintech, China), anti-CAMK2 (1:1000, Cell Signaling Technology, USA), anti-pCAMK2 (1:1000, Cell Signaling Technology, USA), anti-β-actin (1:1000, Cell Signaling Technology, USA), anti-α-tubulin (1:1000, Cell Signaling Technology, USA) and anti-BDNF

(1:1000, Abcam, UK), followed by incubation with anti-rabbit IgG (H+L) (DyLight 800 Conjugate; Cell Signaling Technology, USA) or anti-mouse IgG (H+L) (DyLight 800 Conjugate; Cell Signaling Technology, USA) secondary antibody for 1 hour at room temperature. The bands were visualised with an Odyssey Infrared Imaging System (LI-COR, Lincoln, NE, USA) and analysed with ImageJ (National Institutes of Health, Bethesda, Maryland).

Immunofluorescence staining

The surgical procedures were described previously.[16] Mice were anaesthetised and transcardially perfused continuously with saline and 4% paraformaldehyde (PFA) solution. The brains were collected and postfixed for 24 hours in 4% PFA at 4°C and then dehydrated using 15% and 30% sucrose. Then, 30 μm slices of brain tissues were cut with a microtome (Leica CM1950, Germany). The cultured neurons were fixed with 4% PFA for 20 min and washed three times with PBS. The cells were incubated in 0.5% Triton X-100 for 30 min and blocked with 5% bovine serum albumin for 1 hour at room temperature. Then, cells were incubated overnight at 4°C with primary antibodies, including anti-MAP-2 (1:100, Cell Signaling Technology, USA), anti-pCAMK2 (Thr286) (1:100, Cell Signaling Technology, USA) and anti-βIII-tubulin (1:200, Cell Signaling Technology, USA), followed by secondary antibody incubation for 1 hour. Counterstaining was performed with 40,6-diamidino-2-phenylindole (DAPI; Beyotime, China). Cells were observed under an Olympus confocal laser scanning microscope (Olympus, Tokyo, Japan). Images were analysed with ImageJ software.

Golgi-Cox staining

Animals were anaesthetised and transcardially perfused with saline. Then, their whole brains were immediately removed on ice and placed in a brown glass bottle containing Golgi-Cox solution for fixation and impregnation. The Golgi-Cox solution contained 1% potassium dichromate, 1% mercuric chloride and 0.8% potassium chromate. The brains were stored at 4°C for 14 days, and the Golgi-Cox solution was replaced every 2 days. Afterward, the brains were immersed in a solution of 30% sucrose until they sank. The brains were then cut into 100 μm sections on a vibrating microtome (Leica CM1950, Germany), and the sections were attached to slides and dried. The sections were then dehydrated in 50%, 70%, 95% and 100% alcohol and immersed in CXA (chloroform/xylene/anhydrous ethanol) solution including chloroform, xylene and anhydrous ethanol at a volume ratio of 1:1:1. The sections were cover slipped and photographed by an automatic scanning microscope. The photos were processed using ImageJ software, and the density of dendrite spines was calculated and analysed.

Micro-optical sectioning tomography

Whole mouse brains were placed in a brown glass bottle with Golgi-Cox dye and stained for at least 2 months. Then, the brains were immersed in 1% lithium hydroxide for 24 hours, rinsed in distilled water for 24 hours, sequentially immersed in 50%, 70%, 85%, 95% and 100% alcohol, and 100% alcohol-acetone (1:1) for 2 hours and then transferred to a new brown jar (100% acetone) to dehydrate overnight. After dehydration, the brains were immersed in 50%, 75% and 100% Spurr resin for 8 hours and maintained in 100% Spurr resin for another 8 hours. After polymerisation, the brains were sectioned and imaged at a voxel size of $0.3 \times 0.3 \times 1 \mu m^3$ using the fast micro-optical sectioning tomography (fMOST) system[19] to complete the brainwide data acquisition. Then, the fMOST images were obtained using the BioMapping3000/BioMapping5000 system (Oebio Biological, Wuhan, China). Image preprocessing was implemented using MATLAB and C++. For every brain, three $900 \times 900 \times 900 \mu m$ regions in the perihematomal tissue were reconstructed, and three neuronal cell bodies in each region were traced. Amira software (V.2020.1, FEI, Me'rignac Cedex, France) and Imaris software (V.9.7.2, Bitplane, Switzerland) were used to visualise the data and generate the figures and videos. The filament editor module of Amira was applied to the brainwide tracing of long-range axons in 3D by a combination of automated and manual approaches, and data blocks from the soma along the axons and dendrites were loaded into Amira. The initial and terminal points of fibres in the loaded blocks were assigned, and then Amira automatically calculated the path along which the fibre connected these two points.

Cell culture and treatment

We cultured primary cortical neurons as previously described.[16] Briefly, cortical tissues were dissected from neonatal C57BL/6 mice and cut into pieces ($1 mm^3$), and then the cells were dissociated with 0.125% trypsin (Invitrogen, USA) for 15 min at 37°C. After centrifugation, the cells were resuspended in Dulbecco's modified Eagle medium/Ham's F12 (DMEM/F12; Gibco, USA) supplemented with 10% fetal bovine serum, 1% penicillin/streptomycin and 1% L-glutamine (all from Gibco, USA). Then, the suspension solution was seeded on 24-well and 96-well culture plates, which were coated with 100.0 μg/mL poly-L-lysine (Sigma-Aldrich, USA) and incubated at 37°C in a humidified atmosphere of 5% CO_2. Later, the DMEM/F12 medium was replaced after 4 hours, and 50% of the medium was refreshed every 3 days with maintenance medium, which included neurobasal medium supplemented with 2% B27, 1% penicillin/streptomycin and 1% L-glutamine (all from Gibco, USA).

To simulate experimental ICH in vitro, we added different concentrations of hemin (Sigma-Aldrich, USA) to cells cultured in 96-well culture plates for 24 hours on day 10 of growth and quantified the cell viability by the Cell Counting Kit-8 (CCK-8) assay (Dojindo, Japan). Then, we selected the hemin concentration (40 μM) at which the cell viability was 50%. In addition, the cells were exposed to 0.25 mM or 0.5 mM Hcy (Sigma-Aldrich, USA) or the vehicle for 48 hours. The cells were grouped into the following categories: (a) normal control, (b) hemin

(40 µM), (c) hemin (40 µM) plus Hcy (0.25 mM) and (d) hemin (40 µM) plus Hcy (0.5 mM).

Cell viability assay

The cell viability of cortical neurons was determined using a CCK-8 assay (Dojindo, Japan). To evaluate the ICH model in vitro, the cells were exposed to 0, 10, 20, 30, 40, 50, 60, 70 or 80 µM hemin (Sigma-Aldrich, USA) in 96-well culture plates for 24 hours. Then, 10 µL of CCK-8 solution was added to each well. After incubating for 4 hours at 37°C, the absorbance at 450 nm was measured following the manufacturer's instructions. In addition, the cells were exposed to 0, 0.25, 0.5, 0.75, 1, 1.25 or 1.5 mM Hcy (Sigma-Aldrich, USA) in 96-well culture plates for 48 hours and then quantified.

Transfection experiments

Lentivirus expressing an shRNA targeting pCAMK2A and lentivirus selectively expressing pCAMK2A and calmodulin-dependent protein kinases 2 (CAMK2A) were obtained from GeneChem (Shanghai, China), which were respectively added to cortical neurons to downregulate or upregulate pCAMK2A or CAMK2A. According to the manufacturer's instructions, cells were seeded in the maintenance medium for 24 hours and transfected with lentivirus and HitransG A solution that can promote lentivirus to transfect cells efficiently for 12 hours. As a negative control, the empty vector expressing GFP was used. Then, cells were exposed to hemin (Sigma-Aldrich, USA) for 24 hours at day 10 or Hcy (Sigma-Aldrich, USA) for 48 hours.

Proteome and phosphoproteome
Sample preparation

After being anaesthetised, the mice were transcardially perfused with PBS. For each proteome sample, perihematomal tissue from three mice was collected and mixed, and 40 mg tissue was homogenised using grinding beads (stainless steel, Shanghai Jingxin Industrial Development) on a tissue grinder instrument (Shanghai Jingxin Industrial Development). We used RIPA lysis buffer (50 mM Tris-HCl, pH 7.4, 150 mM NaCl, 0.25% deoxycholic acid, 1% NP-40, 1% SDS) with protease and a phosphatase inhibitor cocktail (HaltTM, Thermo Scientific) for protein extraction. Then, 4 volumes of acetone were added to precipitate proteins for 2 hours at −80°C and the samples were centrifuged for 30 min at 14 000 g. The pellets were then washed two times with 80% acetone. The protein pellets were resuspended in 8 M urea, and a BCA assay was used to determine the protein concentration. Equal masses of protein for each sample were reduced and alkylated by dithiothreitol (final concentration of 10 mM) and iodoacetamide (final concentration of 50 mM) for 1 hour and 45 min, respectively. Then, trypsin (Mass Spectrometry Grade, Promega) was added to the samples at 1:50 (trypsin weight: protein weight) for protein digestion at 37°C overnight. The next day, trypsin was added at 1:100 (trypsin weight: protein weight) and for a 2 hours incubation at 37°C. The digestion was

terminated by adding 10% trifluoroacetic acid (TFA) to adjust the pH to 4. One hundred micrograms of peptides were desalted by an Oasis HLB solid phase extraction (SPE) column (30 µM, Waters), and the remaining digest of approximately 4 mg of peptides was subsequently used for phosphopeptide enrichment.

Phosphopeptide enrichment

The SPE-Ti-IMAC microspheres were purchased from J&K Scientific, Ti(SO4)2 was purchased from Sinopharm Group, and 50 g Ti(SO4)2 and 1 g SPE-Ti-IMAC microspheres were used for the phosphopeptide enrichment of 12 samples. Ti^{4+} was immobilised in the microspheres by the previously reported method[20] to obtain the Ti^{4+}-IMAC material. The material was packed into 1 mL SPE cartridges (30 µM sieve plate) as a Ti^{4+}-IMAC SPE column. The SPE procedure included four common steps: first, the SPE column was washed with 0.1% TFA for three volumes of solid phase, then, the digests were mixed with an equal volume of loading buffer (80% Acetonitrile (ACN)/6% TFA water solution) and loaded onto the column. We then used wash buffer 1 (50% ACN/6%TFA/200 mM NaCl) to remove the nonphosphopeptides on microspheres while wash buffer 2 (30%ACN/0.1%TFA) was used to remove the salt. After the final washing step, elution buffer (10% ammonium solution) was used to elute the phosphopeptides from the microspheres. The elution was evaporated to dryness. Before mass spectrometry (MS) analysis, 1% formic acid (FA) was used to redissolve it.

Liquid chromatography-MS analysis

Peptides of all the proteome samples were separated and analysed on an Easy-nLC 1200 UHPLC (Thermo Fischer Scientific) coupled with a Q Exactive HF-X mass spectrometer (Thermo Fischer Scientific). The trap column was 3 cm×150 µm while the analytical column was 25 cm×150 µm, and both were packed in-house with Repro Sil-Pur C18-AQ (1.9 µm, Dr. Maisch GmbH). A Thermo stainless steel nanobore emitter was used.

The gradient mobile phase was generated by solvent A (0.1% FA) and solvent B (0.1% FA in 80% ACN) at 55°C and applied at a 600 nL/min flow rate for 120 min. The initial mobile phase contained 4% solvent B, and then the fraction of the B phase increased to 7% in 1 min. In the following 94 min, it increased to 25%; after another 16 min, it increased from 25% to 40% and then to 100% after an additional 5 min, where it remained for 4 min.

MS data acquisition was performed in positive ion and data-dependent acquisition modes. All full MS spectra were acquired in a scan range of 350–2000 m/z at a resolution of 60 k. Then, the 20 most intense multiple-charged ions (excluding eight and above) were selected for high energy collision dissociation (HCD) fragmentation and acquired at a resolution of 15 k. The normalised collision energy was 28.

MS data analysis

Raw data files generated from MS analysis were imported into Proteome Discovery software (V.2.4) for protein identification and label-free quantification. The reviewed fasta database of Mus musculus and the common contaminants database were downloaded from UniProt.org (July 2019). Most of the search parameters were set as default, except for the following: carbamidomethylation (+57.021 Da) of cysteine residues was set as a fixed modification; acetylation (+42.011 Da) of the protein N-terminal, oxidation (+15.995 Da) of methionine and phosphorylation (+79.966 Da) of serine, threonine and tyrosine were set as the dynamic modifications.

The mass tolerance for precursor ions was set to 10 ppm and for fragment ions to 0.6 Da. The number of maximum missed cleavage sites was set to 5. All searches were performed in Trypsin/P-specific digestion mode. The false discovery rate was strictly controlled to 0.01 at both the peptide and protein levels. Label-free quantification was used for comparisons between groups.

Data processing and downstream analysis

The protein and peptide (phosphorylation) quantification information was imported into R software (V.4.0.1) for downstream analysis. The *limma* package was used for differential expression analysis. The gene ontology (GO) analyses were performed using the R package *ClusterProfiler. Cytoscape* was used to perform *ClueGO*.[21] To construct the signalome network, kinase–substrate relationship analyses were performed with the R package *PhosR*.

Statistical analysis

All the results are presented as the mean±SE of the mean (SEM) and were statistically analysed using GraphPad Prism V.8.0 (GraphPad Software, San Diego, California). Student's t tests (two-tailed) were used for the single comparisons, and one-way analysis of variances (ANOVAs) were used for the multiple comparisons of data with normal distribution (Shapiro-Wilk tests) and equal variance (F test). The data without normal distribution were analysed by Kruskal-Wallis tests for the multiple comparisons. The repeated-measures ANOVA was used to investigate differences in means across groups with repeated observations over time. When the ANOVA revealed significant differences, post hoc Bonferroni or Dunn's (following Kruskal-Wallis) tests were used to examine pairwise comparisons of means. $p < 0.05$ was considered statistically significant.

RESULTS

Hcy inhibits neurite outgrowth after ICH

According to our study design (online supplemental figure S1), we first explored the effect of Hcy on primary cortical neurons treated with 40 µM hemin, which mimics the phenotype of ICH.[22] The concentrations of hemin and Hcy were determined by CCK8 assay. Approximately 50% of cortical neurons treated with 40 µM hemin and 0.5 mM Hcy survived and the injured neurites gradually recovered (online supplemental figure S2A-B, figure 1A). To assess the neurite outgrowth recovery, the total length, number and mean length of branches were measured. Compared with normal cortical neurons, neurite branches were significantly destroyed 2 days after hemin treated, the total length (187.98±2.94 µm vs 321.94±5.94 µm), the mean length (41.74±0.68 µm vs 54.02±1.16 µm) and the number (3.94±0.07 vs 6.86±0.17) of neurites were significantly decreased (figure 1B–D). In addition, the cortical neurons treated with 40 µM hemin and 0.5 mM Hcy had a worsen morphological indication compared with those treated with 40 µM hemin only at 2 days (total length, 102.92±2.80 µm vs 187.98±2.94 µm; mean length, 35.39±0.83 µm vs 41.74±0.68 µm; the number of branches, 2.80±0.06 vs 3.94±0.07). The neurite outgrowth recovered gradually with time, and the length, number and mean length of cortical neurons treated by hemin only at 4 days were significantly better than those treated by hemin plus Hcy (total length, 271.46±4.01 µm vs 146.46±3.17 µm; mean length, 49.53±0.93 µm vs 44.85±0.80 µm; number of branches, 5.79±0.13 vs 3.46±0.09), meanwhile they were also superior to cortical neurons treated with hemin only at 2 days (total length, 271.46±4.01 µm vs 187.98±2.94 µm; mean length, 49.53±0.93 µm vs 41.74±0.68 µm; number of branches, 5.79±0.13 vs 3.94±0.07). Even though there was an increasing trend of neurite outgrowth between cortical neurons treated with hemin plus Hcy at 4 days and 2 days, there was no significant difference, which means Hcy may impede neurite outgrowth recovery after the attack of ICH. Moreover, Sholl analysis showed that cortical neurons treated with hemin plus Hcy had fewer intersections between the neurites and Sholl circles compared with hemin treated only (figure 1E).

We further investigated the effect of Hcy on neurite outgrowth recovery using a mouse model of ICH with HHcy. The HHcy model was established by feeding mice with a high methionine diet containing 1.7%.[23] After 4 weeks of feeding, the Hcy level of mice fed with high-methionine diet increased fourfold compared with those in an ordinary diet (21.0±4.1 µM vs 5.1±1.1 µM). The ICH model was induced after 6 weeks of high-methionine diet, and the concentration of Hcy exceeded 70 µM (online supplemental figure S2C). We evaluated the volume of haematoma using T2-weighted imaging (online supplemental figure S2D), and there was no significant difference between ICH mice plus high-methionine diet (HHcy+ICH) and ICH mice plus ordinary diet (Ctrl+ICH). To evaluate the neurite outgrowth recovery at a global level, modified whole-brain Golgi staining and a micro-optical sectioning tomography (MOST) system were used to acquire the fine structure of neurons.[24] Neurons of the caudoputamen, hippocampal formation and basolateral amygdalar nucleus were reconstructed (figure 1F). We collected the neurite branch density in different brain regions, which was calculated by dividing the total length of neurites and the volume of different reconstructed regions (figure 1G–I). Still, the same trends persisted in animal models compared 14 days with 3 days, while the neurite branch density in HHcy+ICH was significantly less than
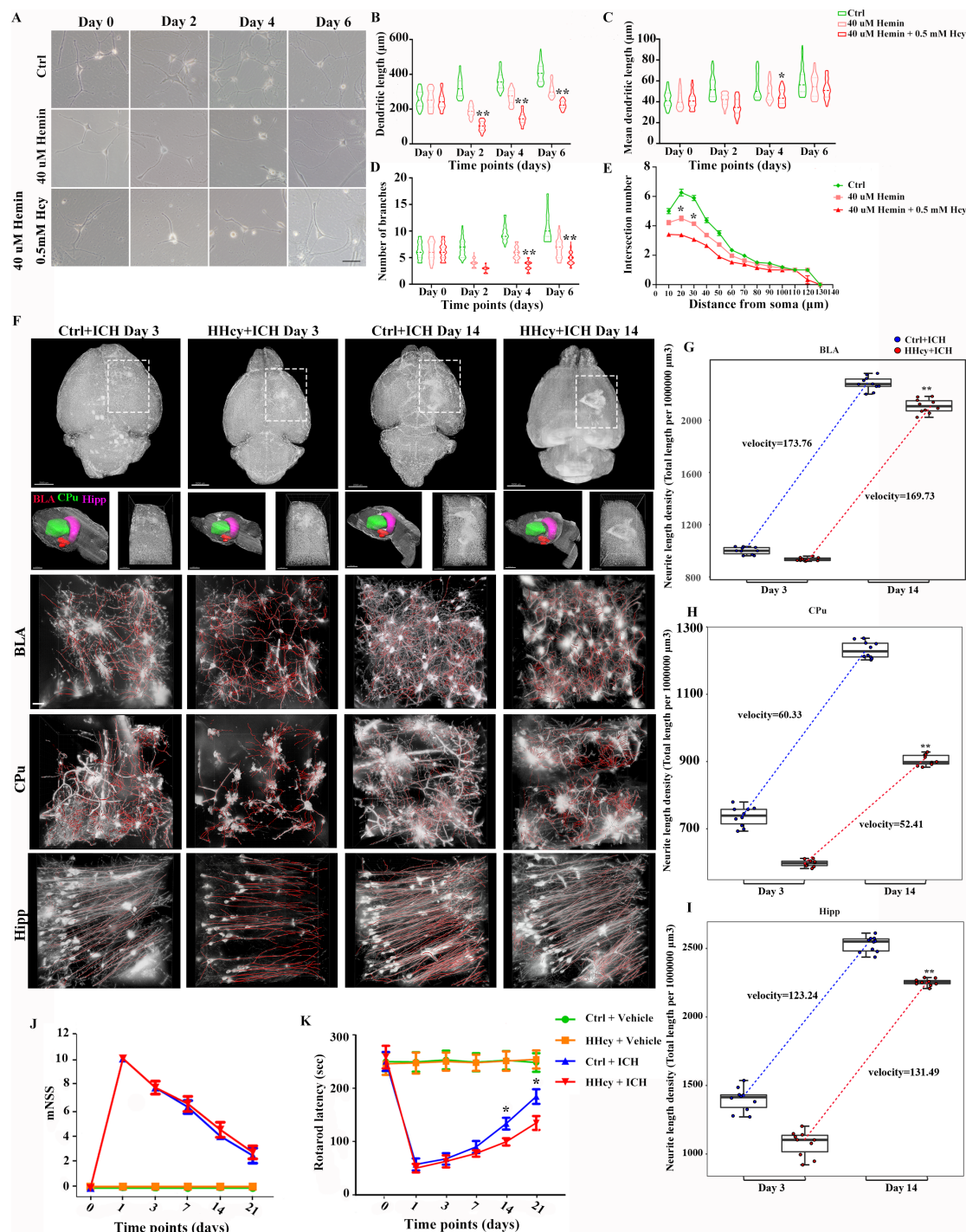
Figure 1 Hcy impedes neurite outgrowth after ICH in vitro and in vivo. (A) Primary cortical neurons were treated with hemin only or combined with Hcy. Cells were observed at different time points under a light microscope. The total length of neurites (B), the mean length of neurites (C) and the number of branches of neurites (D) were measured. n=50~120/group. (E) Sholl analysis for neurite complexity at day 6. n=50~120/group. *p<0.05, **p<0.01, 40μM hemin versus 40μM Hemin+0.5mM Hcy treatment in B) through E). (F) Representative 3D reconstruction pictures of mouse brains by MOST in the HHcy+ICH and Ctrl+ICH groups on days 3 and 14, respectively. Row 3, 4 and 5: Detail 'blocks' in the Basolateral amygdalar nucleus (BLA), Caudoputamen (CPu) and Hippocampal formation (Hippo). Row 1: bar=2000μm; row 2: bar=1500μm; row 3–5: bar=40μm. (G–I), Neurite branch length density: total length of neurite branches in the block/the volume of the block. n=10/group. **p<0.01, HHcy+ICH group vs Ctrl+ICH group. Neurological function was assessed using a modified Neurological Severity Score (J) or Rotarod test (K). n=8/group. *p<0.05, HHcy+ICH group versus Ctrl+ICH group. Statistical significance was calculated with the two-tailed unpaired Student's t tests in (B) through (E), one-way ANOVA/Tukey's tests or Kruskal-Wallis tests in (G) through (I) and Mann-Whitney U tests in (J) and K). Data are presented as the mean±SEM. ANOVA, analysis of variance; Ctrl, control; Hcy, homocysteine; HHcy, hyperhomocysteinemia; ICH, intracerebral haemorrhage; MOST, micro-optical sectioning tomography.

Ctrl+ICH group at 3 days and 14 days after ICH. Additionally, the velocity of the neurites branches density increased was calculated by dividing the changes of neurite branch density between different times and time intervals, the HHcy+ICH group had a reduced velocity. Moreover, neurological functional outcomes at different time points were evaluated using the mNSS and rotarod test (figure 1J–K). An increase in mNSS and a decrease in rotarod latency occurred in the ICH model, and the neurological function after ICH gradually recovered with the progress of time, which was characterised by a reduction of the mNSS score and an increase in rotarod latency. Also, the defect of neurological function in HHcy+ICH was significantly more serious than Ctrl+ICH group at 14 days and 21 days after ICH. To verify the differences in neurite outgrowth recovery between HHcy+ICH and Ctrl+ICH group, the quantification of microtubule-associated protein-2 (MAP-2) and synaptophysin protein expression levels was detected by western blot (online supplemental figure S2E-G), which are the markers of neurites.[25 26] The expression of MAP-2, a marker of neurons, was significantly reduced in HHcy+ICH mice 14 days after ICH compared with that of Ctrl+ICH mice. Meanwhile, the expression level of synaptophysin showed the same trend. Both cellular and animal models show that Hcy inhibits neurite outgrowth after ICH.

Hcy strongly alters the phosphorylation status of proteins associated with neurite outgrowth after ICH

To investigate the precise mechanisms of Hcy on neurite outgrowth, label-free proteome and IMAC-based phosphoproteome were acquired and analysed (figure 2A). We identified a total of 3348 proteins and 3188 phosphoproteins, meanwhile, overlapping data from phosphoproteome and proteome profiling revealed 1924 proteins (figure 2B). Figure 2C,D represented the protein and phosphoprotein levels across different groups. A total of 256 proteins and 69 phosphoproteins were found to be significantly altered in HHcy+ICH group compared with Ctrl+ICH group, while only seven proteins changed both their levels and phosphorylation levels (figure 2E, online supplemental table 1,2). GO enrichment analysis was carried out on upregulated and downregulated (phospho)proteins. The levels of proteins associated with actin filament organisation (GO:0007015), animal organ regeneration (GO:0031100) and positive regulation of response to wounding (GO:1903036) were downregulated significantly in HHcy+ICH group compared with Ctrl+ICH group, meanwhile, downregulated phosphoproteins by Hcy mainly were associated with regulation of actin filament depolymerisation (GO:0030834) and regulation of supramolecular fibre organisation (GO:1902903). The changes in actin filament are important to neurite outgrowth.[27] In contrast, there were no significantly enriched biological pathways for the upregulated proteins or phosphoproteins by Hcy after ICH.

Kinase substrate analysis reveals that CAMK2A plays an important role in Hcy-induced phosphorylation disturbance

Uncovering potential kinase-substrate pairs hidden in the phosphoproteome is important for interpreting the underlying biological significance of phosphoproteome data. Here, by using a multistep kinase-substrate scoring method reported by Yang et al,[28 29] a signalome was constructed to identify discrete protein modules with similar kinase regulation and phosphorylation profiles. According to the signalome data (figure 3A–C), five distinct modules (1, 2, 3, 4 and 5) existed across four groups. Moreover, the signalome map highlighted that module 5 was entirely regulated by Ca^{2+}/CAMK2A and that the others were coregulated by several kinases. Most phosphosites of module 5 were downregulated in HHcy+ICH group (online supplemental figure S3), and gene set enrichment analysis (GSEA) revealed that module 5 was significantly associated with signalling for regulation of cell shape and neuron projection maintenance (figure 3D). These findings suggest that phosphorylation of CAMK2A may be a key molecular switch for neurite outgrowth, which was turned off by Hcy after ICH.

### Hcy significantly downregulates the phosphorylation level of CAMK2A after ICH

The results of previous proteomics and phosphoproteomics studies revealed that Hcy might regulate the CAMK2A kinase-substrate group (figure 3, online supplemental figure S3). Thus, we examined the levels of CAMK2A and phospho-CAMK2A on the third-day post-ICH through the western blot (figure 4A–E). The western blot data showed that the level of pCAMK2A and pCAMK2B was increased in the Ctrl+ICH group compared with that in the Ctrl+vehicle group at 3 days and that the level decreased under HHcy treatment. However, no significant difference was found in the expression level of CAMK2A among HHcy+ICH group and Ctrl+Vehicle group (figure 4A–E). Additionally, after cortical neurons were treated with hemin for 24 hours and cultured with different concentrations of Hcy for 48 hours, decreased phosphorylation level of CAMK2A was observed through immunofluorescence staining (figure 4F–G).

Considering that brain-derived neurotrophic factor (BDNF) is a key downstream target of CAMK2 to promote neurite outgrowth,[30] we detected the expression level of BDNF by western blot (figure 4H–I). Results showed that Hcy significantly downregulated BDNF levels after ICH.

Upregulation of CAMK2A reverses the inhibition of neurite outgrowth after ICH by Hcy

To further explore the value of pCAMK2A as a potential therapeutic target for promoting neurite outgrowth after ICH with HHcy, lentivirus expressing a shRNA targeting pCAMK2A and lentivirus selectively expressing pCAMK2A and CAMK2A were obtained, which were used to downregulate or upregulate pCAMK2A or CAMK2A. According to immunofluorescence staining data (figure 5A–D), the length and number of neurite branches were significantly
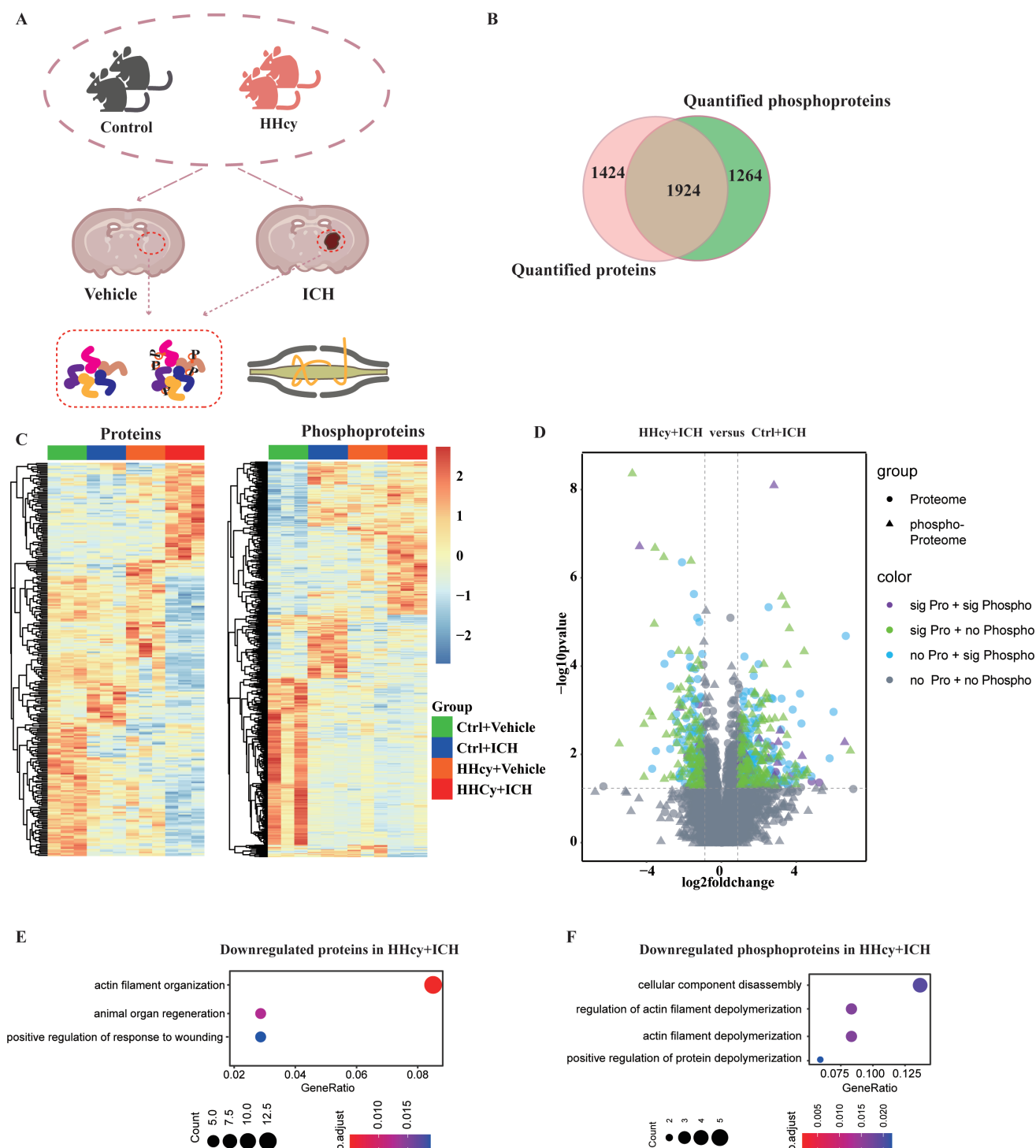
Figure 2 Hcy downregulates proteins and phosphoproteins associated with neurite outgrowth. (A) Flowchart of the experimental design to collect proteome and phosphoproteome. (B) The overlap relationships between proteins and phosphoproteins detected by LC-MS/MS. (C) Heatmaps reveal differently expressed proteins and phosphoproteins analysis among groups. The colour bar represents the expression levels. (D) Volcano plot of proteome and phosphoproteome data. Data are represented as log (2) fold change for the HHcy+ICH group compared with that of the Ctrl+ICH group. The origins represent levels of proteins from the proteome, and small triangles represent the phosphoprotein levels. The colour of the dots represents the significance levels of proteins and phosphoproteins. Purple dots, sig Pro+sig Phospho, the proteins are both significantly changed in the proteome and phosphoproteome; green dots, no Pro+sig Phospho, the proteins are significantly changed in phosphorylation levels, but there were no significant changes in protein levels; sky blue dots, the proteins are significantly changed in protein levels, but there were no significant changes in phosphoprotein levels; grey dots, there were no significant changes in the proteome and phosphoproteome. GO enrichments for proteins (E) and phosphoproteins (F) downregulated in HHcy+ICH versus Ctrl+ICH groups. Ctrl, control; GO, gene ontology; Hcy, homocysteine; HHcy, hyperhomocysteinemia; ICH, intracerebral haemorrhage; LC-MS/MS, liquid chromatograph mass spectrometer.
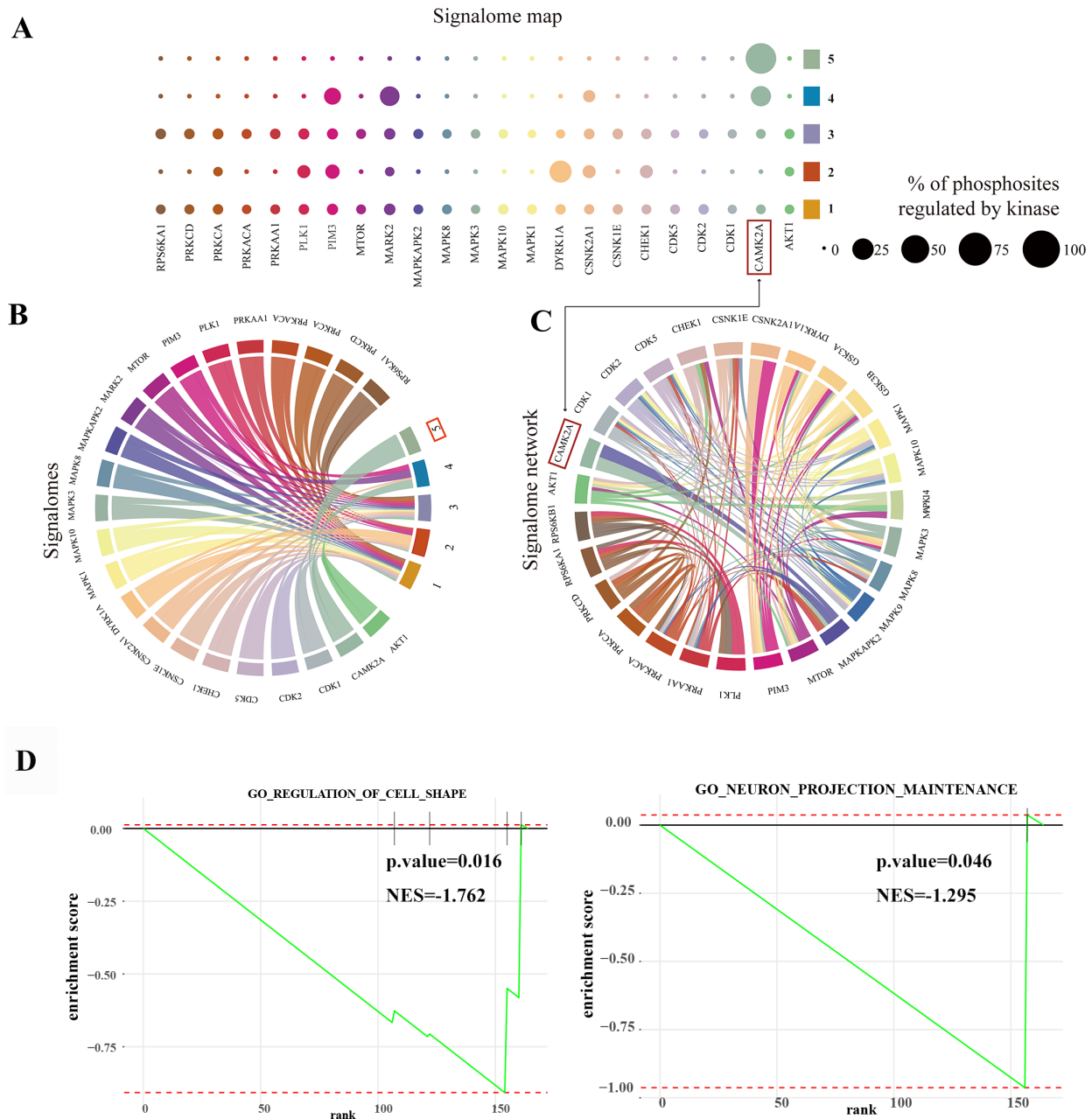
Figure 3 Construction of the signalome across different groups using the phosphoproteome. (A,B) The signalome map identified 23 kinases that make up the branches, and five phosphosite modules consisted of the stem nodes with a distinct regulatory profile. The bubble chart displays the proportion of phosphosite modules regulated by different kinases. Module 5 was fully regulated by CAMK2A. (C) A network of interactions among kinases. (D) The changes between HHcy+ICH and Ctrl+ICH were enriched by gene sets enrichment analysis. Ctrl, control; HHcy, hyperhomocysteinemia; ICH, intracerebral haemorrhage; NES, normalised enrichment score.

reduced when exposed to hemin and Hcy compared with those of hemin treatment alone. Interestingly, the elevated protein or phosphorylation levels of CAMK2A increased the length and number of neurite branches. This finding suggests that CAMK2A plays an important role in neurite outgrowth after ICH. Meanwhile, on reducing the level of phosphorylated CAMK2A, the complexity of neurites was comparable to that of the cotreatment group with hemin and Hcy. These results suggest that pCAMK2A may be a potential target to promote neurite outgrowth in convalescent patients with ICH with HHcy.

DISCUSSION

In the present study, we found that Hcy could impede neurite outgrowth and neurological function recovery after ICH. Using the quantitative phosphoproteome together with a global proteome analysis, we revealed for the first time that Hcy affected the protein phosphorylation alterations associated with neurite outgrowth. Through in vitro and in vivo experiments, we confirmed that Hcy significantly inhibited neurite outgrowth after ICH through decreasing phosphorylation of CAMK2A. This is the first study to report the inhibitory effect of
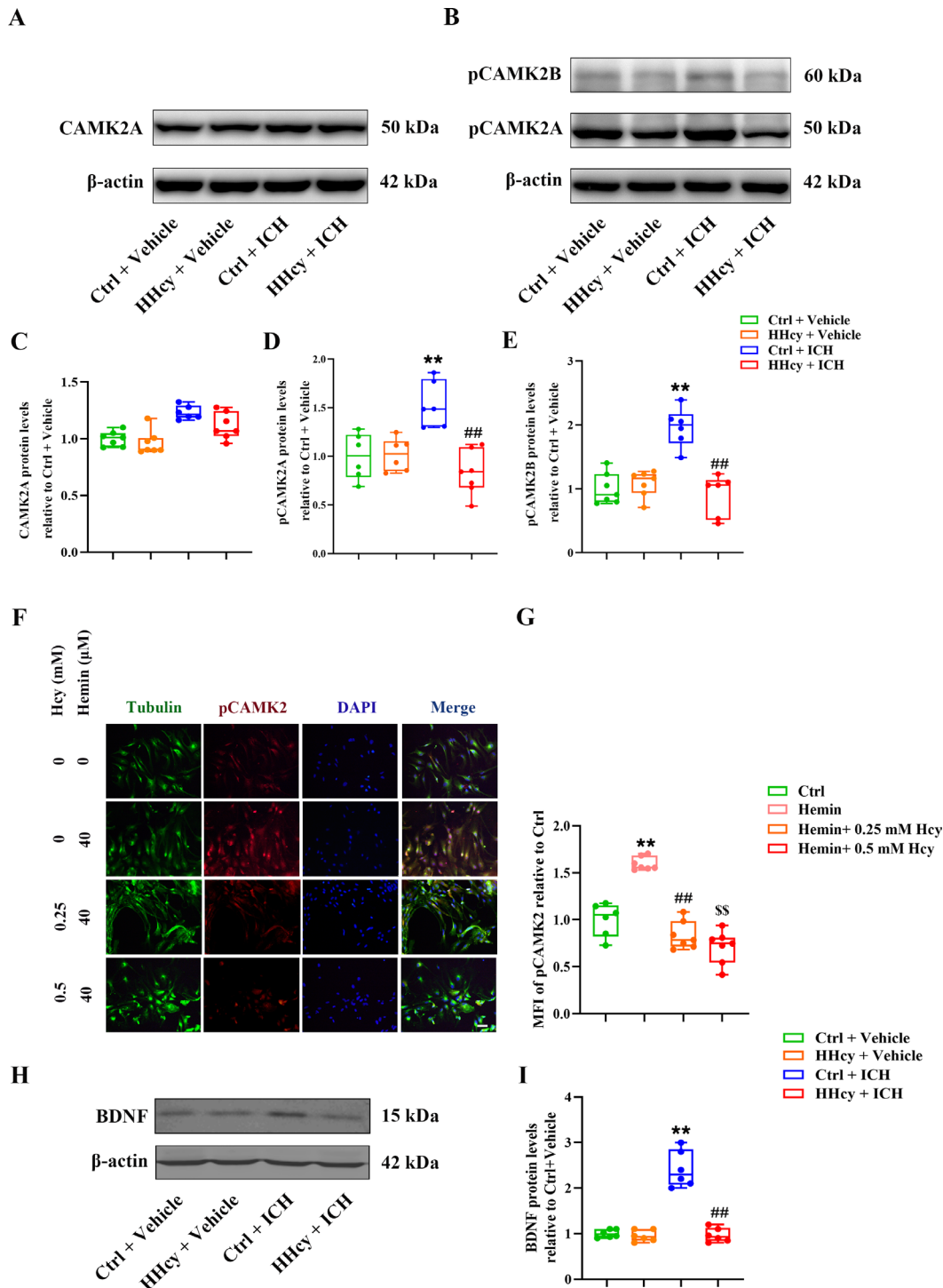
Figure 4 Hcy significantly downregulates the phosphorylation level of CAMK2A after ICH. (A,B) Total CAMK2, phosphorylated (p) CAMK2A and pCAMK2B were detected by Western blot in the Ctrl+Vehicle, HHcy+Vehicle, Ctrl+ICH and HHcy+ICH groups on day 3. (C) through (E) Quantification of CAMKII, p-CAMK2A and p-CAMK2B protein expression levels relative to the Ctrl+Vehicle group by Western blot. n=6~7/group. (F) After exposure to hemin for 24 hours and two concentrations of Hcy for 48 hours, cortical neurons were assessed by immunofluorescence with pCAMK2 (red), β-tubulin III (green), and DAPI (blue) staining. Scale bar=50 μm. (G) Quantification of the MFI of pCAMK2 from (F). n=6~7/group. (H) BDNF was detected by Western blot in the Ctrl+Vehicle, HHcy+Vehicle, Ctrl+ICH and HHcy+ICH groups on day 3. (I) Quantification of BDNF protein expression levels relative to the Ctrl+Vehicle group from (H) is shown. n=6/group. Statistical significance was calculated with one-way ANOVA/Tukey's tests or Kruskal-Wallis tests in (C) through (E), (G) and (I). Data are presented as the mean±SEM **p<0.01, Ctrl+ICH group versus Ctrl+Vehicle group; ##p<0.01, HHcy+ICH group versus Ctrl+ICH group in (C) through (E) and (I). **p<0.01, 40 μM Hemin group versus Ctrl group; ##, $$p<0.01, 40 μM Hemin+0.25 mM or 0.5 mM Hcy group versus 40 μM Hemin group in (G). ANOVA, analysis of variance; Ctrl, control; Hcy, homocysteine; HHcy, hyperhomocysteinemia; ICH, intracerebral haemorrhage; MFI, mean fluorescence intensity.
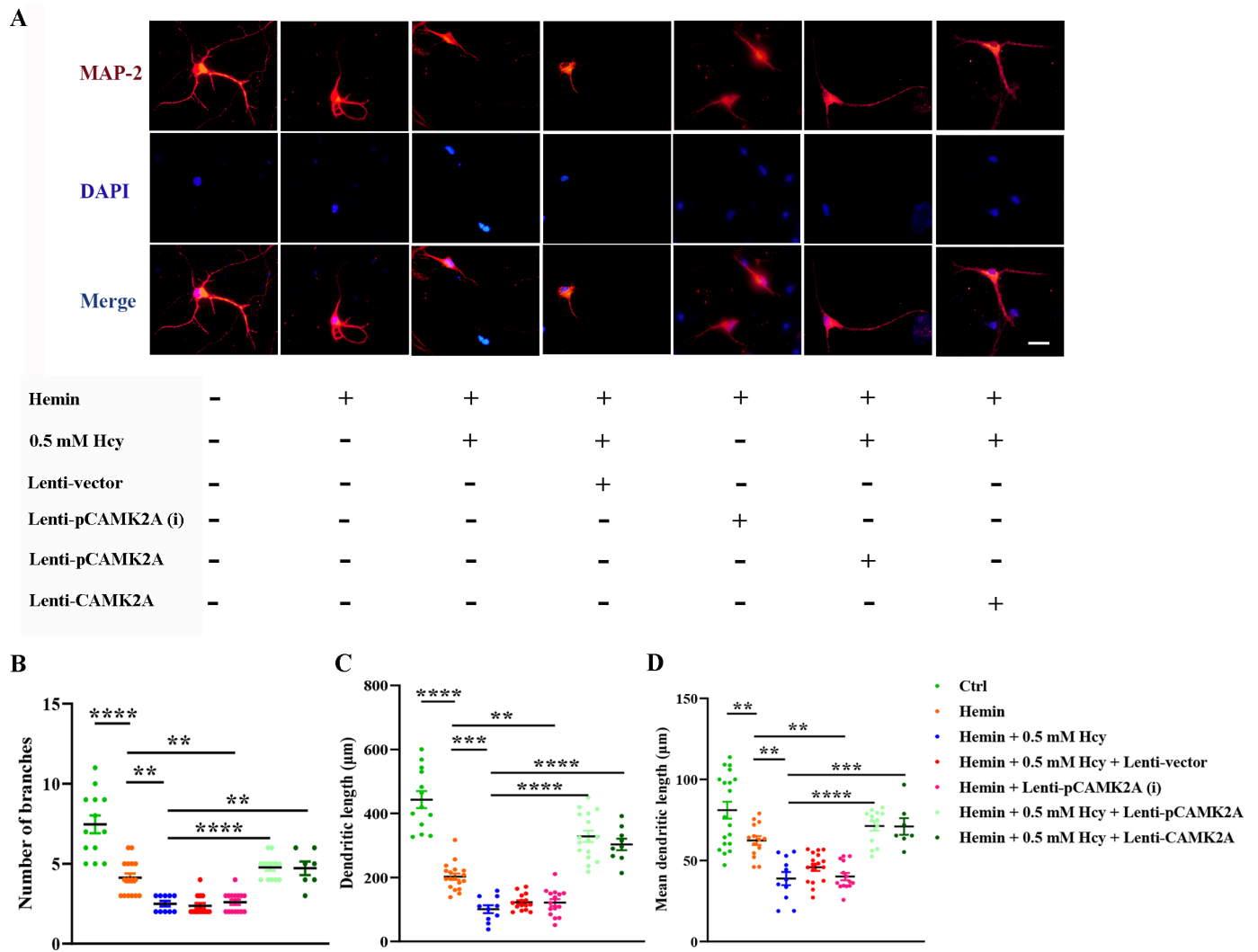
Figure 5 Upregulation of pCAMK2A reverses the inhibition of neurite outgrowth after ICH by Hcy. (A) After exposure to hemin for 24 hours and Hcy (0.5 mM) for 48 hours, cortical neurons treated with Lenti-pCAMK2A(i), Lenti-pCAMK2A and Lenti-CAMK2A for 12 hours were assessed by immunofluorescence with MAP2 (red) and DAPI (blue) staining. Lenti-pCAMK2A(i) treatment downregulated the level of pCAMK2A by mutating protein phosphorylation site (S286) to positively charged alanine, Lenti-pCAMK2A treatment upregulated the level of pCAMK2A by mutating protein phosphorylation site (S286) to negatively charged aspartic acid. Scale bar=50 μm. The number of branches of neurites (B), the total length of neurites (C) and the mean length of neurites (D) were measured. n=7~19/group. Statistical significance was calculated with the one-way ANOVA/Tukey's tests or Kruskal-Wallis tests in (B) through (D). Data are presented as the mean±SEM **p<0.01, ***p<0.001, ****p<0.0001. ANOVA, analysis of variance; Ctrl, control; Hcy, homocysteine; ICH, intracerebral haemorrhage.

Hcy on neurite outgrowth recovery after ICH and the underlying mechanisms of this process. Accordingly, by promoting neurite outgrowth, pCAMK2A is a potential therapeutic target for patients with ICH with HHcy.

Elevated plasma concentration of Hcy, a sulfur-containing amino acid, has been shown in observational (cohort and case-control) studies and systematic reviews to be a potential risk factor for vascular diseases and stroke in particular. Reduction in Hcy levels is significantly associated with a reduced risk of first stroke,[31] and high Hcy levels can predict higher recurrence and mortality in ischaemic stroke, especially in patients with the large-vessel atherosclerosis subtype.[32 33] Experimental studies have also confirmed that HHcy has an impact on cerebral vascular biology, and its molecular mechanisms

include oxidative stress, proinflammatory pathways and endothelial dysfunction.[34] Additionally, Wang *et al* found that Hcy enhanced neural stem cell autophagy in in vivo and in vitro models of ischaemic stroke, which may be one of the molecular mechanisms of Hcy neurotoxicity.[35] In addition, elevated plasma Hcy concentration is associated not only with ischaemic stroke but also with haemorrhagic stroke. Several studies have shown that HHcy is independently associated with a higher risk of ICH, a larger haematoma volume, a poorer prognosis and a lower survival rate in patients with ICH.[4 6 36–38] Neuroinflammation and the increased activity of the matrix metalloproteinase 2 (MMP2) and MMP9 systems induced by HHcy may underlie the pathogenesis of ICH.[39] Moreover, in our study, by using morphological and behavioural

experiments, we found more serious neurological deficits and decreased neurites branches density in ICH mice treated with HHcy (figure 1). Therefore, Hcy can inhibit neurite outgrowth recovery in ICH models, which may be one of the reasons for poor prognosis.

There is growing evidence that the protein phosphorylation induced by protein kinases is one of the primary mechanisms involved in the regulation of signal transduction pathways that control neurite outgrowth in the mammalian brain and, thus, affects motor control, sensory processing and synaptogenesis.[40–42] Protein tyrosine kinases and many common serine/threonine kinases, such as cyclic adenosine monophosphate (cAMP)-dependent protein kinase, CAMK2 and Ca^{2+}/phospholipid-dependent protein kinase, are highly expressed in the central nervous system.[40 42] Protein kinases can influence dendritic growth to form synaptic contacts and regulate neurite plasticity through the phosphorylation of specific substrates, and, thus, the dysregulation of kinases may perturb dendritic growth and synaptic function and lead to disease states.[43] Therefore, it is necessary to use the quantitative phosphoproteome together with a global proteome analysis to further explore the mechanism by which HHcy impedes neurite outgrowth recovery during ICH. We showed that several kinase families, such as CAMKs and mitogen-activated protein kinases, drive the changes in phosphosites caused by HHcy during ICH (figures 2 and 3). Moreover, among the related kinase families, we found that CAMK2A activity may be largely responsible for the inhibition of neurite outgrowth recovery mediated by Hcy (figures 4 and 5).

CAMK2, a Ser/Thr protein kinase, is critical in Ca^{2+} signal transduction and is highly enriched at the synapses in the brain tissue.[44] There are four isoforms of CAMK2 (α, β, γ and δ) encoded by four distinct but highly related genes (CAMK2A, CAMK2B, CAMK2G and CAMK2D).[45] Among them, the α and β isoforms of CAMK2 are the most abundant isoforms expressed in neurons[46] and CAMK2A has been identified as a central regulator of neuronal plasticity.[45] After Ca^{2+} enters the cell through N-methyl-D-aspartate receptors and binds to calmodulin (CaM), Ca^{2+} alters its conformation, and Ca^{2+}/CaM binds to CAMK2 to activate it by autonomous phosphorylation at T286 (on CAMK2B) or Thr287 (on CAMK2B), and this process contributes to many neuronal regulatory pathways.[46 47] The substrates phosphorylated by CAMK2 include proteins that modulate presynaptic transmission as well as essential plasticity-regulating receptors and signalling molecules in the postsynaptic cells.[44] CAMK2 regulates presynaptic plasticity by limiting synaptic vesicle release.[46] One study reported that peripheral axon injury increased the phosphorylation level of CAMK2 and that activation of CAMK2-promoted neuronal axon growth in vitro, which demonstrates that CAMK2 is a critical modulator of mammalian axon regeneration.[48] In addition, CAMK2 is important for dendrite development and dendritic spine formation.[43] We showed that the levels of most phosphorylation sites of the CAMK2A substrate in ICH mice treated with HHcy were significantly lower than those of the control group, indicating that Hcy might regulate the CAMK2A kinase-substrate group and inhibit neurite outgrowth recovery. Furthermore, we found that pCAMK2A levels were upregulated in ICH mice and in vitro with hemin treatment. Through an experiment utilising primary neurons treated with hemin, Hcy and lentiviruses, we showed that the upregulation of CAMK2A and pCAMK2A expression reduced the inhibitory effect of Hcy on neurite outgrowth recovery and that the downregulation of pCAMK2A levels suppressed neurite outgrowth recovery in vitro with hemin treatment. Thus, based on our results, it is possible that the expression of pCAMK2A is upregulated in ICH but reduced by Hcy, and this may be the mechanism by which Hcy inhibits neurite outgrowth recovery and neurological recovery. Additionally, the nerve growth factor and neurotrophic drugs can stimulate nerve regrowth,[49] and BDNF signalling via its transmembrane receptor tropomyosin-related kinase B is essential for neuronal survival, differentiation and axonal growth.[50 51] Studies have shown that CAMK2 can induce phosphorylation of cAMP response element-binding protein (CREB), which binds to a cAMP response element within genes and alters the expression of key proteins involved in neurite outgrowth, such as BDNF.[52–54] Consistently, our results indicated that Hcy could inhibit the expression of BDNF in the perihematomal region after ICH (figure 4H,I). Therefore, we speculate that Hcy may inhibit neurite outgrowth through the CAMK2/BDNF pathway, which will be further explored in our subsequent study. However, our study had the limitation that in vivo experiments were not conducted to verify the effects of upregulation or downregulation of CAMK2A and pCAMK2A expression on neurite outgrowth recovery and neurological function in ICH mice. In addition, given the importance of elevated neurogenesis in the subventricular zone (SVZ) after stroke for neurological recovery,[55] we examined whether Hcy affects neurogenesis in the SVZ after ICH. We used immunofluorescence to assess the expression level of doublecortin (DCX) in the SVZ after ICH, which is normally expressed on NPCs and is considered a marker of neurogenesis in adulthood.[56] We found that the percentage of DCX+cells in the SVZ after ICH was significantly lower in the Hcy+ICH group than in the Ctrl+ICH group, indicating that Hcy might inhibit neural rehabilitation by suppressing neurogenesis after ICH, which needs further in-depth study (online supplemental figure S4).

In conclusion, our results demonstrate that Hcy can downregulate the levels of pCAMK2A and CAMK2 kinase-substrate group during ICH, which explains why Hcy inhibits neurite outgrowth in vivo and in vitro. This study may provide direct evidence for the potential of novel therapeutic targets to manage the neurotoxic effect of Hcy in patients with ICH with high Hcy levels.

ORCID iDs
Yuming Xu http://orcid.org/0000-0003-2689-9897
Zhouping Tang http://orcid.org/0000-0002-4153-8590

REFERENCES

1. Krishnamurthi RV, Feigin VL, Forouzanfar MH, *et al*. Global and regional burden of first-ever ischaemic and haemorrhagic stroke during 1990-2010: findings from the global burden of disease study 2010. *Lancet Glob Health* 2013;1:e259–81.
2. Cordonnier C, Demchuk A, Ziai W, *et al*. Intracerebral haemorrhage: current approaches to acute management. *Lancet* 2018;392:1257–68.
3. Xi G, Keep RF, Hoff JT. Mechanisms of brain injury after intracerebral haemorrhage. *Lancet Neurol* 2006;5:53–63.
4. Li Z, Sun L, Zhang H, *et al*. Elevated plasma homocysteine was associated with hemorrhagic and ischemic stroke, but methylenetetrahydrofolate reductase gene C677T polymorphism was a risk factor for thrombotic stroke: a multicenter case-control study in China. *Stroke* 2003;34:2085–90.
5. Ahmed S, Bogiatzi C, Hackam DG, *et al*. Vitamin B 12 deficiency and hyperhomocysteinaemia in outpatients with stroke or transient ischaemic attack: a cohort study at an academic medical centre. *BMJ Open* 2019;9:e026564.
6. Wang D, Wang W, Wang A, *et al*. Association of severity and prognosis with elevated homocysteine levels in patients with intracerebral hemorrhage. *Front Neurol* 2020;11:571585.
7. Weiss N, Heydrick S, Zhang Y-Y, *et al*. Cellular redox state and endothelial dysfunction in mildly hyperhomocysteinemic cystathionine beta-synthase-deficient mice. *Arterioscler Thromb Vasc Biol* 2002;22:34–41.
8. Signorello MG, Segantin A, Passalacqua M, *et al*. Homocysteine decreases platelet no level via protein kinase C activation. *Nitric Oxide* 2009;20:104–13.
9. Shirafuji N, Hamano T, Yen S-H, *et al*. Homocysteine increases tau phosphorylation, truncation and oligomerization. *Int J Mol Sci* 2018;19:891.
10. Haberberger RV, Barry C, Matusica D. Immortalized dorsal root ganglion neuron cell lines. *Front Cell Neurosci* 2020;14:184:184.:.
11. Park SY, An JM, Seo JT, *et al*. Y-27632 induces neurite outgrowth by activating the nox1-mediated Akt and PAK1 phosphorylation cascades in PC12 cells. *Int J Mol Sci* 2020;21:7679.
12. Shah DI, Singh M. Possible role of Akt to improve vascular endothelial dysfunction in diabetic and hyperhomocysteinemic rats. *Mol Cell Biochem* 2007;295:65–74.
13. Bao W-D, Zhou X-T, Zhou L-T, *et al*. Targeting mir-124/ferroportin signaling ameliorated neuronal cell death through inhibiting apoptosis and ferroptosis in aged intracerebral hemorrhage murine model. *Aging Cell* 2020;19:e13235.
14. Xiong X-Y, Liu L, Wang F-X, *et al*. Toll-Like receptor 4/myd88-mediated signaling of hepcidin expression causing brain iron accumulation, oxidative injury, and cognitive impairment after intracerebral hemorrhage. *Circulation* 2016;134:1025–38.
15. Chen J, Li Y, Wang L, *et al*. Therapeutic benefit of intravenous administration of bone marrow stromal cells after cerebral ischemia in rats. *Stroke* 2001;32:1005–11.
16. Pan C, Liu N, Zhang P, *et al*. Egb761 ameliorates neuronal apoptosis and promotes angiogenesis in experimental intracerebral hemorrhage via rsk1/gsk3β pathway. *Mol Neurobiol* 2018;55:1556–67.
17. Wang X, Liu D, Huang H-Z, *et al*. A novel microrna-124/ptpn1 signal pathway mediates synaptic and memory deficits in alzheimer's disease. *Biol Psychiatry* 2018;83:395–405.
18. Li G, Yu H, Liu N, *et al*. Overexpression of CX3CR1 in adipose-derived stem cells promotes cell migration and functional recovery after experimental intracerebral hemorrhage. *Front Neurosci* 2019;13:462.
19. Li A, Gong H, Zhang B, *et al*. Micro-optical sectioning tomography to obtain a high-resolution atlas of the mouse brain. *Science* 2010;330:1404–8.
20. Yao Y, Dong J, Dong M, *et al*. An immobilized titanium (IV) ion affinity chromatography adsorbent for solid phase extraction of phosphopeptides for phosphoproteome analysis. *J Chromatogr A* 2017;1498:22–8.
21. Shannon P, Markiel A, Ozier O, *et al*. Cytoscape: a software environment for integrated models of biomolecular interaction networks. *Genome Res* 2003;13:2498–504.
22. Cheng J, Tang J-C, Pan M-X, *et al*. L-lysine confers neuroprotection by suppressing inflammatory response via microrna-575/pten signaling after mouse intracerebral hemorrhage injury. *Exp Neurol* 2020;327:113214.
23. Suszyńska-Zajczyk J, Luczak M, Marczak L, *et al*. Hyperhomocysteinemia and bleomycin hydrolase modulate the expression of mouse brain proteins involved in neurodegeneration. *J Alzheimers Dis* 2014;40:713–26.
24. Guo C, Long B, Hu Y, *et al*. Early-stage reduction of the dendritic complexity in basolateral amygdala of a transgenic mouse model of alzheimer's disease. *Biochem Biophys Res Commun* 2017;486:679–85.
25. Bodakuntla S, Jijumon AS, Villablanca C, *et al*. Microtubule-associated proteins: structuring the cytoskeleton. *Trends Cell Biol* 2019;29:804–19.
26. Veschsanit N, Yang J-L, Ngampramuan S, *et al*. Melatonin reverts methamphetamine-induced learning and memory impairments and hippocampal alterations in mice. *Life Sci* 2021;265:118844.
27. Ciaffardini F, Nicolai S, Caputo M, *et al*. The Cockayne syndrome B protein is essential for neuronal differentiation and neuritogenesis. *Cell Death Dis* 2014;5:e1268.
28. Yang P, Humphrey SJ, Cinghu S, *et al*. Multi-omic profiling reveals dynamics of the phased progression of pluripotency. *Cell Syst* 2019;8:427–45.
29. Kim HJ, Kim T, Hoffman NJ, *et al*. PhosR enables processing and functional analysis of phosphoproteomic data. *Cell Rep* 2021;34:108771.
30. Yan X, Liu J, Ye Z, *et al*. Camkii-Mediated CREB phosphorylation is involved in Ca2+-induced BDNF mRNA transcription and neurite outgrowth promoted by electrical stimulation. *PLoS One* 2016;11:e0162784.
31. Huang X, Li Y, Li P, *et al*. Association between percent decline in serum total homocysteine and risk of first stroke. *Neurology* 2017;89:2101–7.
32. Shi Z, Liu S, Guan Y, *et al*. Changes in total homocysteine levels after acute stroke and recurrence of stroke. *Sci Rep* 2018;8:6993.
33. Shi Z, Guan Y, Huo YR, *et al*. Elevated total homocysteine levels in acute ischemic stroke are associated with long-term mortality. *Stroke* 2015;46:2419–25.
34. Faraci FM, Lentz SR. Hyperhomocysteinemia, oxidative stress, and cerebral vascular dysfunction. *Stroke* 2004;35:345–7.
35. Wang M, Liang X, Cheng M, *et al*. Homocysteine enhances neural stem cell autophagy in in vivo and in vitro model of ischemic stroke. *Cell Death Dis* 2019;10:561.
36. Zhou Z, Liang Y, Qu H, *et al*. Plasma homocysteine concentrations and risk of intracerebral hemorrhage: a systematic review and meta-analysis. *Sci Rep* 2018;8:2568.

37 Zhou F, Chen B, Chen C, *et al*. Elevated homocysteine levels contribute to larger hematoma volume in patients with intracerebral hemorrhage. *J Stroke Cerebrovasc Dis* 2015;24:784–8.

38 Li Q, Zhao Z, Si K, *et al*. Correlation between the levels of NLRP3, hcy, IL-1β, IL-18 and the prognosis in patients with hemorrhagic stroke. *Am J Transl Res* 2021;13:2883–90.

39 Sudduth TL, Powell DK, Smith CD, *et al*. Induction of hyperhomocysteinemia models vascular dementia by induction of cerebral microhemorrhages and neuroinflammation. *J Cereb Blood Flow Metab* 2013;33:708–15.

40 Raymond LA, Blackstone CD, Huganir RL. Phosphorylation of amino acid neurotransmitter receptors in synaptic plasticity. *Trends Neurosci* 1993;16:147–53.

41 Hawasli AH, Bibb JA. Alternative roles for Cdk5 in learning and synaptic plasticity. *Biotechnol J* 2007;2:941–8.

42 Huganir RL, Greengard P. Regulation of neurotransmitter receptor desensitization by protein phosphorylation. *Neuron* 1990;5:555–67.

43 Nourbakhsh K, Yadav S. Kinase signaling in dendritic development and disease. *Front Cell Neurosci* 2021;15:624648.

44 Hudmon A, Schulman H. Neuronal Ca2+/calmodulin-dependent protein kinase II: the role of structure and autoregulation in cellular function. *Annu Rev Biochem* 2002;71:473–510.

45 Nicole O, Pacary E. Camkiiβ in neuronal development and plasticity: an emerging candidate in brain diseases. *Int J Mol Sci* 2020;21:7272.

46 Moro A, van Woerden GM, Toonen RF, *et al*. Camkii controls neuromodulation via neuropeptide gene expression and axonal targeting of neuropeptide vesicles. *PLoS Biol* 2020;18:e3000826.

47 Sałaciak K, Koszałka A, Żmudzka E, *et al*. The calcium/calmodulin-dependent kinases II and IV as therapeutic targets in neurodegenerative and neuropsychiatric disorders. *Int J Mol Sci* 2021;22:4307.

48 Xi F, Xu R-J, Xu J-H, *et al*. Calcium/Calmodulin-Dependent protein kinase II regulates mammalian axon growth by affecting F-actin length in growth cone. *J Cell Physiol* 2019;234:23053–65.

49 Chen L, Chen T, Mao G, *et al*. Clinical neurorestorative therapeutic guideline for brainstem hemorrhage (2020 china version). *Journal of Neurorestoratology* 2020;8:232–40.

50 Esvald E-E, Tuvikene J, Sirp A, *et al*. Creb family transcription factors are major mediators of BDNF transcriptional autoregulation in cortical neurons. *J Neurosci* 2020;40:1405–26.

51 Harward SC, Hedrick NG, Hall CE, *et al*. Autocrine BDNF-TrkB signalling within a single dendritic spine. *Nature* 2016;538:99–103.

52 Sheng M, Thompson MA, Greenberg ME. CREB: A ca(2+)-regulated transcription factor phosphorylated by calmodulin-dependent kinases. *Science* 1991;252:1427–30.

53 Tao X, Finkbeiner S, Arnold DB, *et al*. Ca2+ influx regulates BDNF transcription by a CREB family transcription factor-dependent mechanism. *Neuron* 1998;20:709–26.

54 Shieh PB, Hu SC, Bobb K, *et al*. Identification of a signaling pathway involved in calcium regulation of BDNF expression. *Neuron* 1998;20:727–40.

55 Zhao Y, Guan Y-F, Zhou X-M, *et al*. Regenerative neurogenesis after ischemic stroke promoted by nicotinamide phosphoribosyltransferase-nicotinamide adenine dinucleotide cascade. *Stroke* 2015;46:1966–74.

56 Couillard-Despres S, Winner B, Schaubeck S, *et al*. Doublecortin expression levels in adult brain reflect neurogenesis. *Eur J Neurosci* 2005;21:1–14.